RotCFD - A Tool for Aerodynamic Interference of Rotors: Validation and Capabilities

R. Ganesh Rajagopalan
rajagopa@iastate.edu
Iowa State University
Ames, IA

Venkat Baskaran, Andrew Hollingsworth, Angela Lestari
Sukra Helitek, Inc.
Ames, IA

Daniel Garrick
Iowa State University
Ames, IA

Eduardo Solis
Monterey Technologies, Inc.
Monterey, CA

Brandon Hagerty
Universities Space Research Association
Moffett Field, CA

Abstract

A novel design tool called RotCFD has been developed at Sukra Helitek, Inc. At conceptual and preliminary rotorcraft design stages, an analysis tool is successful only if problem set-up time is minimal and run times are economical. In addition, during detailed design stages, often times, additional design questions arise that need answers in a reasonable time. The above requirements led to the genesis of RotCFD which is based on its predecessor Rot3DC. RotCFD attempts to bridge the two worlds of design and Computational Fluid Dynamics (CFD) with the help of an Integrated Design Environment (IDE) specific to rotorcraft. RotCFD emphasizes user-friendliness and efficiency that streamline the design process from geometry to CFD solution. The key components of RotCFD are a geometry module, a semi-automated grid generation module, a flow-solver module, a rotor module, a flow visualization and analysis module, all integrated in one environment. The concept of rotor blades represented by momentum sources forms the basis of this aerodynamic simulation tool for rotorcraft. The rotor momentum sources are primarily a function of the local velocity of the flow and the two-dimensional airfoil characteristics of the rotor blades. The Navier-Stokes equations and the blade element theory are coupled implicitly to yield a self-contained method for generating performance, as well as the near and far wake including all the aerodynamic interference inherent in a situation. The method has been subjected to a set of well known cases and the results compare well with available data. The current capabilities of this unique tool, its components and preliminary validation results are presented.

Introduction

During initial design studies, parametric variation of vehicle geometry is routine. The paradigm of RotCFD follows the concept of Integrated Design Environment (IDE), specific to rotorcraft. Rotorcraft engineers traditionally use the wind tunnel to evaluate and finalize designs. The existence of wind tunnel walls do influence the testing environment from actual free air conditions, since the flow behavior changes near the tunnel walls. Correlation between wind tunnel results and flight tests, when not good, have been often attributed in part to uncertainty in blockage corrections. Estimation of rotor blockage is significantly more complex than bluff body corrections as the correction depends on operational characteristics such as rotor RPM and thrust produced. In addition to being a design tool, RotCFD allows simulation of a

[0]Presented at the American Helicopter Society Future Vertical Lift Aircraft Design Conference, January 18-20, 2012, San Francisco, California,

complete rotorcraft configuration with or without wind tunnel walls including all the facility effects. The key principle in the development of the architecture is to make the environment user friendly, robust and easy to learn. Often times the nature of any computational solution is that multiple tools are required that begin with geometry manipulation to post-processing, analysis and visualization of the simulated results. RotCFD provides a rudimentary set of tools for all the steps a rotorcraft design engineer needs to computationally simulate a rotorcraft and analyze the simulation. To make the tool user friendly an intuitive Graphical User Interface (GUI) has been developed and is available on popular operating systems such as Mac, Windows and Linux. The software has been designed to give the same look and feel in all the platforms supported. The robustness of the tool is enabled by semi-automating the process of grid generation with minimal user input. The learning experience is made easy by providing judicious defaults and requiring a small number of initial inputs for a simple rotor case. The underlying CFD algorithm is based on a pressure based algorithm SIMPLE[1] known for its robustness and suitability to low speed flows. The simplicity and robustness are possible because the rotor is modeled using momentum sources; individual blades are not modeled in the computational simulation. Two-dimensional airfoil tables specific to the rotor blades are required for obtaining a proper solution. Currently, the automated body-conforming grid generation does not produce grids suitable for a viscous solution. RotCFD is based on Rot3DC, a structured single-zone Cartesian grid solver. The current version of RotCFD is a mixed-element unstructured hanging-node solver. In summary, RotCFD is an Integrated Design Environment (IDE) specific to rotors which can simulate a complete rotorcraft with or without wind tunnel walls. At the heart of the innovation are:

1. A Graphical User Interface (GUI), with user friendly and intuitive input and output menus, that interacts with all the components of the software and is the front end to the capabilities of the tool.
2. A minimal CAD-like geometry engine to manipulate multiple bodies and rotors.
3. An automated hybrid grid generator that produces nearly conforming grids around the bodies and unstructured Cartesian grids everywhere else.
4. A robust and economical incompressible flow solver for the entire system of grids.
5. Momentum source based rotor model for simulating configurations with multiple rotors.
6. A flow visualization tool for CFD post-processing.

The sections that follow briefly describe the theory, the architecture, and the implementation details of the GUI; the geometry engine; the grid generator; the flow solver; and the post-processing tools natively available in RotCFD for visualizing the results. In addition, a set of validation cases have been developed and preliminary results are presented.

RotCFD the Tool

In this section, the various components of the RotCFD tool are described.

RotCFD GUI Architecture: The RotCFD GUI acts as the front-end to all the processes of the IDE. The GUI is also designed to be used for different types of flow solvers and applications. Central to the design of the architecture of RotCFD is the commonality of most flow solvers and rotor problems.

- Geometry preparation and manipulation.
- The steps involved in running different processes specific to the simulation.
- The data required as input to the solvers.
- The tools used to visualize the results and post process the simulation.

The GUI is where the particular problem or scenario is defined: the geometry is loaded, the rotor and flow properties are defined, the grid is generated, and the solver is started. The GUI is also where one visualizes the geometry, the grids, and the solution. Many of these steps and tools are common to all the different types of grid generators and solvers within RotCFD. Some of these basic commonalities are:

- The ability to load, manipulate, and visualize geometry (including rotors)
- The ability to load and visualize grids
- The ability to load and visualize solutions

Much of this common functionality is part of what is called the RotCFD Project Shell or simply the "Shell." All projects are derived from the functionalities in the Shell. The Shell consists of two main

parts: a visualization manager (on the left, Fig. 1) and an object manager (on the right, Fig. 1). The visualization manager is used to visualize the RotCFD objects: bodies, rotors, grids, and solutions. The object manager contains a list of the above objects, and each one of these objects can be selected to reveal a number of properties in the properties area to allow manipulation of the objects. Not only does this allow many different applications to share the same tools, it also enforces a common look and feel across all applications.

Shell includes base C++ classes for all geometry objects. These classes have the ability to load, perform basic transformations, and draw the geometry in the visualization manager. Hence all projects can load and place geometry in any location and orientation, and view that geometry relative to other geometries and the boundary. Shell also includes base classes and tools that are used for any grid and any solution. These classes and tools are used to visualize grids and solution data and perform simple tasks such as generating contour lines for solutions.

The GUI allows the data entered to be saved as a single file to the disk in what is known as the project file. Project files are saved in such a way that they can be opened, as the same project or as a different project type (using the "Open As" menu item in the File menu) and modified and saved. This allows the commonality between input to different type of projects used as default values. For example a helicopter project file read in as input to a tilt rotor project will load all the information it recognizes and have all the common information filled in such as the value for free stream velocity.

Geometry Module: During initial design studies, parametric variation of vehicle geometry is routine. A simple geometry tool (modest CAD functionality) is offered to simplify geometry manipulation. The current version of RotCFD can read the body geometry in STL or Plot3D format. Also, some simple shapes (bodies of revolution) can be generated from within RotCFD. In addition to general transformations such as translation, rotation and scaling, parametric variation of the geometry is available to assist with the design. Graphical visualization is used to make the geometry manipulation user-friendly: the user is able to see a preview of the geometry change before committing the change. Figure 2 depicts the NASA Large Civil Tilt-Rotor configuration in the CAD tool. A preview of the geometry after a scaling factor of 2.0 is shown in Fig. 3 before the scaling is actually applied. The blue lined box indicates the original size before scaling. The geometry can also be duplicated and then translated to compose a group formation, such as shown in Fig. 4. Each individual aircraft can be transformed, as is seen in Fig. 5 where the rear aircraft is rotated to the left.

UGen: Body Conforming Grid Generator: The internal grid generator is referred to as UGen in RotCFD. UGen can be a stand-alone module or a sub-process of another application. UGen generates an octree grid as the volume grid which grows from the outer boundaries of the domain and intersects the body (if there exists one). The Cartesian unstructured (hanging node) grid is economical to generate and can be completely automated. The cells that intersect the body, and all the cells that immediately surround the intersected cells are replaced by tetrahedra. The simple shape of the tetrahedron allows the grid to be morphed slightly in order to conform to the body. Thus the body conforming grid generator modifies a Cartesian octree grid (Cartesian here meaning all faces are aligned with the Cartesian planes) such that the grid will approximately conform to the surface of the body. The grid is approximate since the algorithm only considers the intersections between the surface geometry and the edges of the original grid. New surface faces are generated based on those edge-surface intersections instead of using the original polygons from the surface geometry. This approximate approach avoids the technical difficulties associated with maintaining the surface geometry exactly as it intersects the grid, and allows the development of a simpler, and more robust algorithm with a much shorter development time. The approach also has the advantage that clean geometries are not required, only that they be closed surfaces.

The body conforming grid generation algorithm moves vertices that are close to the surface to surface-edge intersections slightly distorting the shape of cells. In order to avoid distorting the cells too much, vertices are limited to how far they can be moved. In instances where edge intersections are not close enough to any of the adjacent vertices, the edge is split and a new vertex is added on the surface intersection instead of moving any of the vertices. The basic outline of the body-conforming grid generation algorithm follows:

1. Starting with a Cartesian octree grid, all the

cells that intersect the geometry, and all the cells that immediately surround the intersected cells are sub-divided into tetrahedra.

2. The edges of the grid are then intersected with the surface geometry.

3. The vertices of the grid that are close to an intersection on an adjacent edge are marked to be moved to the closest intersection.

4. An edge that has an intersection that is not near any of its adjacent vertices is split at the intersection point.

5. Any split edge may lead to the creation of additional surface edges, faces and cells.

6. Vertices marked to be moved are moved.

7. Interior cells are removed.

The resulting surface representation within the grid will approximate the original CAD surface of the input geometry to roughly the same fidelity as the grid refinement. Geometry features that are much larger than the grid cells will be well approximated, features of the same order as the size of the grid cells will be roughly approximated, and features much smaller than the size of the grid cells will likely be lost. It is illustrative to show an example of this process in 2-D. The left side of Fig. 6 shows a continuous curve running through a 2-D grid. The intersections are marked as dots, arrows indicate to which intersection the original grid vertices will be moved, and circled intersection dots indicate intersection points that will not be included in the final grid but will be collapsed into the nearby moved vertex. The right side of Fig. 6 shows the modified grid. This can help give a sense of how the cells are modified, and how the approximation of the curve is of the order of the length of the edges.

Flow Solver: The flow field of a rotor is complex. Even an isolated rotor is dominated by the mutual, aerodynamic interference effects of the blades. Therefore, all simulation techniques, to be successful, must consider interference effects. Any numerical algorithm that solves the Navier-Stokes equations is adequate for obtaining the flow field. The SIMPLER/SIMPLE [1] line of pressure based algorithms are suitable for low speed flows and currently SIMPLE is used for solving the flow field in RotCFD. The three-dimensional unsteady, generalized transport equation for a scalar ϕ can be written in the conservation form as:

$$\frac{\partial}{\partial t}(\rho\phi) + \nabla \cdot \left(\rho\vec{V}\phi\right) = \nabla \cdot (\mu \nabla\phi) + S_\phi \qquad (1)$$

where μ is the diffusion coefficient and S_ϕ is the source term including the rotor sources. The four terms in the transport equation are the unsteady, convection, diffusion and source terms.

Integrating Eqn. 1 for the time interval from t to $t + \Delta t$ about a general control volume $\Delta\forall$, shown in Fig. 7 gives:

$$\int_t^{t+\Delta t}\int_{\Delta\forall}\frac{\partial}{\partial t}(\rho\phi)\,d\forall dt + \int_t^{t+\Delta t}\int_{\Delta\forall}\nabla\cdot\rho\vec{V}\phi d\forall dt = \int_t^{t+\Delta t}\int_{\Delta\forall}\nabla\cdot\mu\nabla\phi d\forall dt + \int_t^{t+\Delta t}\int_{\Delta\forall}S_\phi d\forall dt \qquad (2)$$

Time variation of a general variable ϕ is given by the generalized formula

$$\int_t^{t+\Delta t}\phi dt = \left[\alpha\phi + (1-\alpha)\,\phi^\circ\right]\Delta t \qquad (3)$$

where ϕ° is the value at the old time step t and ϕ is the value at the new time $t + \Delta t$. The parameter α makes the scheme fully explicit, fully implicit or partially implicit. In particular, $\alpha = 0$ leads to an explicit scheme, $\alpha = 0.5$ leads to a Crank-Nicolson scheme and $\alpha = 1$ leads to a fully implicit scheme.

Integrating about each face, f, of the control volume $\Delta\forall$ and using the time integral Eqn. 3, Eqn. 2 is discretized as follows:

$$\frac{\left[(\rho\phi) - (\rho\phi)^\circ\right]}{\Delta t}\Delta\forall + \alpha\sum_f\left(\rho\vec{V}\phi\right)\cdot\vec{A} + (1-\alpha)\sum_f\left(\rho\vec{V}\phi\right)^\circ\cdot\vec{A} = \alpha\sum_f(\mu\nabla\phi)\cdot\vec{A} + (1-\alpha)\sum_f(\mu\nabla\phi)^\circ\cdot\vec{A} + \alpha S_\phi\Delta\forall + (1-\alpha)\,S_\phi^\circ\Delta\forall \qquad (4)$$

Equation 4 can be evaluated for any given control volume to find the fluxes across the faces. More details of the SIMPLER algorithm and its application to the unstructured solver used in RotCFD are available in Refs.[1], [2] and [3]. Of particular interest is

the term S_ϕ in the above equations through which the rotor is modeled.

Rotor Modeling: The concept of rotor blades represented by momentum sources forms the basis of the rotor modeling. The momentum source algorithm (Refs. [4, 5, 6]) used in RotCFD has been tested and validated and is central to the simplifications and efficiency inherent in RotCFD. The Navier-Stokes equations and the blade element theory are coupled implicitly to yield a self-contained method for generating unsteady performance, as well as the near and far wake including all the aerodynamic interferences present. The classical blade element theory yields the correct forces on the rotating blades once the local vector velocity field is known. The numerical algorithm that solves the Navier-Stokes equations provides the flow field near the rotor blades which also includes the rotor induced momentum sources. The two-dimensional airfoil characteristics of the rotor blades and the local velocity of the flow are the basis for the computation of the momentum sources. Thus, when the momentum equations converge the rotor sources and hence the forces on the blades also have converged implicitly yielding the rotor performance and flow field.

Results

The results presented in this section are grouped in three categories: (a) Solver Validation, (b) Rotor Performance Validation and (c) Rotor-Body Interference Validation. The choice of the validation cases used are largely based on publically available experimental data. The rotor results presented depend to a significant degree on the airfoils used and the kinematic conditions of the experimental setup. Where possible, the results have also been compared to Rot3DC, the first generation software of RotCFD, which has been validated and used quite extensively for many practical applications. Representative cases are presented for each one of the above categories. All the case studies presented here are simulated using commonly available personal computers and most of the post-processing was done using the visualization module within the RotCFD GUI.

Solver Validation: The 3-D lid driven cavity is chosen here as a standard validation case for the flow solver. The solver is used for vortex-filled rotor flows and the 3-D lid driven cavity exhibits a characteristic swirling flow at the center. The boundary conditions of this flow confined to the cavity are simple to set up. Without loss of generality, the directional bias of the solver, if there exists any, can be tested easily and hence was chosen for this study. The cavity is a unit cube with $L = 1\ m$ and the lid (top plane) is moving with a constant velocity of 1 m/s. No-slip boundary condition is applied on all the other boundaries. The movement of the lid drives the flow inside due to the transport of shear stress by molecular viscosity. $Re = (\rho U_{lid} L/\mu)$ is the flow Reynolds number, where ρ is the fluid density and μ is the fluid viscosity. The cavity flow is simulated for a Reynolds number of 400 for grid sizes (22 x 22 x 22), (42 x 42 x 42), (62 x 62 x 62) and (82 x 82 x 82). The cases are simulated with the well-validated Rot3DC as well as with RotCFD, where an equivalent unstructured grid is used. For the Reynolds number of 400, the velocity profile of 'u' on the vertical centerline is shown in Fig. 8. The computed results converge to the reference solution with successive grid refinements. Overall good agreement between Rot3DC and RotCFD results is shown.

Rotor Performance: Two model helicopter rotors in hover are chosen for the purpose of validating the ability of RotCFD to predict rotor performance. The first rotor is the model helicopter rotor tested by Caradonna and Tung [7]. The second test case is the Rabbot rotor from Ref. [8]. The test conditions are given in Table 1 and the important geometric parameters for these rotors are given in Table 2. Both are untwisted rotors with no flapping. The rotor from Ref. [7] has a cone of $\frac{1}{2}^o$ and the rotor from Ref. [8] has no cone. The same cases were simulated using the Rot3DC solver with a comparable grid. Where data is available, RotCFD results are compared with the results from Rot3DC and measurements.

Rotor-I, Ref. [7]: A cross plane view of the grid used in the simulation is shown in Fig. 9. The grids get finer and finer as they get close to the rotor without refining the rest of the domain. The variation of coefficient thrust (C_T) with time is shown in Fig. 10. The performance of the rotor converges rather early in the time history and shows minimal variation there after. This trend is very common for the momentum source approach and thus, if performance prediction is the goal, simulation times can be shortened accordingly. Table 3 compares the predicted values of C_T for RotCFD, Rot3DC and the experiment. Fig. 11 depicts the correlation of the thrust coefficient with the collective pitch. The performance results from RotCFD compare well with the Rot3DC results for a wide range of collective pitch angles.

Rotor-II, Ref. [8]: A C_T sweep for a range of collective

pitch angles is simulated and presented for Rotor-II, from Ref. [8], in Table 4. Good agreement between the RotCFD and Rot3DC predictions is observed. An important feature of a good rotor model is its capability to accurately predict the loading on rotor blades. Figure 12 depicts the radial aerodynamic loading for a collective pitch of 4.5^o. A good agreement is observed between RotCFD and the experiment. The mismatch in the outboard region of the blade is a result of using uncorrected 2-D airfoil data for the blade elements near the tip where three-dimensional effects are dominant. For a rotor in hover, Figure of Merit (FM) is an important parameter that defines the efficiency of the rotor. FM calculated for Rotor-II at various C_T values is compared to Rot3DC results as well as the experimental values in Fig. 13.

The total thrust produced by a rotor and the torque required to generate this thrust are important considerations in designing the rotor and any analysis tool should be able to predict them. Figure 14 presents the variation of the thrust coefficient C_T with the blade collective pitch θ_c. Since experimental data is not available for very high values of θ_c, a comparison is made over a moderate range of blade pitch angles and the expected linear increase of C_T with the collective pitch is observed. In Fig. 15, RotCFD predicted variation of the thrust coefficient with the coefficient of torque compares well with the experimental data. The C_T and C_Q values are averaged over 50 rotor rotations.

In addition to the rotor performance, qualitative information about the flow field is characterized for the isolated rotor tests. Figure 16 shows the instantaneous pressure contours around Rotor-II and the velocity vectors for a collective pitch angle of 4.5^o. The expected pressure differential across the rotor is observed, with high pressure below and low pressure above, thereby maintaining the correct physics of a rotor flow. The presence of the tip vortex is also discernible at the rotor tip. Figure 17 shows the instantaneous velocity magnitude contours on the rotor plane, while Fig. 18 shows the instantaneous rotor wake on an x-plane passing through the rotor center. The contraction of the flow through the rotor is observed. Also the influence of the rotor is confined to a narrow region below the rotor.

Rotor-Body Interference Studies: Two simple bodies are considered for analyzing the aerodynamic interference of the rotor and the fuselage. The first body is a geometric shape that has a cylindrical body with a hemispherical nose region. This body shape is simple and yet has complex flow structures. This validation case is based on data from Ref. [9]. The second geometry is the generic fuselage shape known as the Robin body from Mineck [10]. Robin is a more representative fuselage shape and yet can be analytically represented. To the extent possible the input to RotCFD is based on the experimental setup and what is available in the open literature.

Georgia Tech Body: This validation case is based on data from Ref. [9] and Ref. [11]. The primary objective of this test case is to compare the calculated pressure coefficient distributions on top, bottom, advancing side, and the retreating side of the body with the experimental data provided in the report. An advance ratio of 0.1 is selected for this validation simulation. The rotor and airframe geometric properties are given in Table 5. The flapping harmonics are represented by $\beta = \beta_0 + \sum_{n=1}^{N} \beta_{nc} \cos(n\psi) + \beta_{ns} \sin(n\psi)$. The rotor blade pre-coning angle is set equal to the zero-flapping harmonic coefficient (β_0). Forward flight test conditions are given in Table 6. A schematic of the geometry is presented in Fig. 19. The grid for this case was automatically generated by RotCFD upon specifying the domain, the number of cells and the refinement regions. Different views of the grid are presented in Figs. 20 and 21. The pressure coefficient (C_P), defined as $C_P = \frac{p - p_\infty}{\frac{1}{2}\rho V_\infty^2}$, distribution on top of the isolated airframe (without the rotor) at a free stream velocity of 33.169 ft/s is presented in Fig. 22. The measured C_P distribution shows a dip near $X/R = 1$ probably due to the support structure hanging from above not modeled in the current analysis. Next, the solution for the combined rotor and body geometry for $\mu = 0.1$ is discussed. An isometric view of the velocity vectors in the Y-plane through the rotor center is depicted in Fig. 23. The vectors represent the components of velocity in this plane while the color of the vectors is a function of all the three components of the velocity, namely the velocity magnitude as indicated in the color bar, the legend. The impingement of the rotor wake on the body is well captured. Cp distributions on the top, bottom, advancing and retreating sides of the body are given in Figs. 24, 25, 26, and 27 respectively. The Cp distribution on the top surface of the body in Fig. 24 shows the double peak illustrating the rotor wake impingement as seen in Fig. 23. The data extraction technique for the body pressure from the CFD solution for this mixed element solver within

RotCFD is at best experimental and there is room for improvements in the overall quality of the results.

Robin Body: The primary objective of this test case is to compare the C_P distributions at different stations along the body longitudinal axis (X axis) with the experimental data from Ref. [10]. The rotor geometric properties are given in Table 7. A schematic from Ref. [10] is given in Fig. 28. An advance ratio of 0.151 is selected for this validation study and the RotCFD results are compared with the corresponding wind tunnel results for conditions listed in Table 8. The grid for this case was automatically generated by RotCFD upon specifying the domain, the number of cells and the refinement regions. The grid-body intersection at $\frac{X}{l} = 0.35$, where l=0.5*body length, along the body axis is shown in multiple views in Fig. 29 and Fig. 30. An isometric view of the body pressure from RotCFD rotor-body simulation is depicted in Fig. 31. A comparison between RotCFD results and the wind tunnel experiment are presented next. All of this information is obtained through the visualization tools of the RotCFD GUI. C_P distribution comparisons for section-cuts at $\frac{X}{l} = 0.35$ and $\frac{X}{l} = 1.35$ are given in Figs. 32 and 33 respectively. The agreement is reasonable.

As an illustration of the capabilities of the software for analyzing multi-body interference effects, RotCFD simulation results for the NASA LCTR aircraft parked (rotors turning) near a terminal are portrayed in Fig. 34 and Fig. 35. The extent of the flow interaction and the characteristics of the aerodynamic interaction are obvious.

Future Work

Upon consideration of the capabilities and the current limitations of the software certain possible extentions can be enumerated.

1. Unsteady rotor (individual blade modeling).
2. Rotor trim.
3. Viscous body-conforming grid.
4. Turbulence modeling.
5. Maneuvering rotors.
6. Parallelization of the solver to take advantage of multi-processor computing.

Summary

RotCFD is an Integrated Design Environment (IDE) specific to rotors that can simulate a complete rotorcraft with or without wind tunnel walls. At the heart of the IDE are:

1. A Graphical User Interface (GUI) with user friendly and intuitive input and output menus.
2. A minimal CAD like geometry engine to manipulate the body.
3. An automated hybrid grid generator with nearly conforming grids around the bodies and unstructured Cartesian grids everywhere else.
4. A robust and economical incompressible flow solver for the entire system of grids.
5. Momentum-source based rotor model for simulating configurations with multiple rotors.
6. A flow visualization tool for CFD post-processing.

The limited validation studies presented here show that RotCFD can be used for studying rotor performance, flow field, and interference effects at the early stage of the design using commodity hardware.

Acknowledgments

The authors have been privileged to have worked with many distinguished people from the rotor community who contributed technically and financially to the development of this method and their contributions are recognized here: William Warmbrodt, Gloria Yamauchi, Larry Young, Euan Hooper, Chuck Keys, Tony McVeigh, Leo Dadone, John Liu, Ram JanakiRam, Hormoz Tadghighi, Tom Maier, Frank Caradonna, Bob Ormiston, Roger Strawn, Chee Tung, John Berry, Marvin Moulton and Bob Moffitt.

The authors acknowledge the help given by the Sukra team Pavithra Premaratne, Kanchan Guntupalli and Luke Novak during the writing of this paper, without which this work could not have been completed.

This work was funded by NASA SBIR Contract Numbers NNX11CD08P and NNX09CA03C.

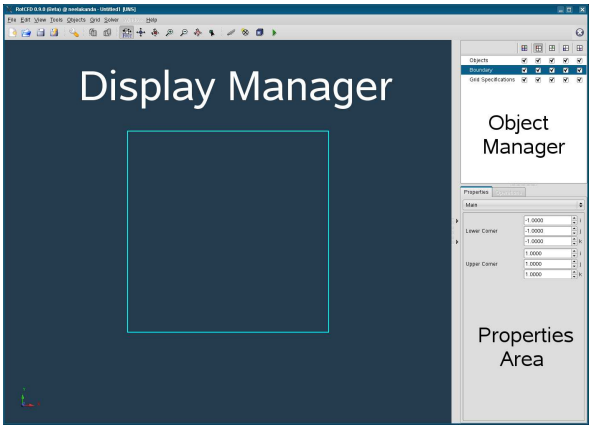

Figure 1: The Project Shell.

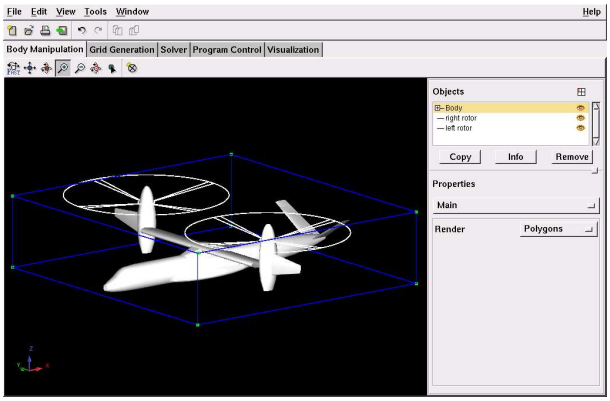

Figure 2: LCTR geometry in the geometry tool.

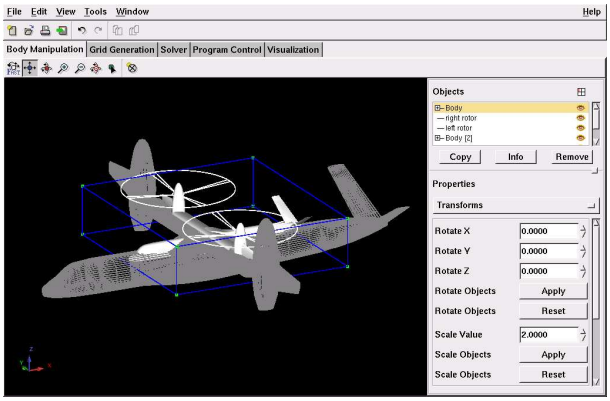

Figure 3: Preview of scaled geometry.

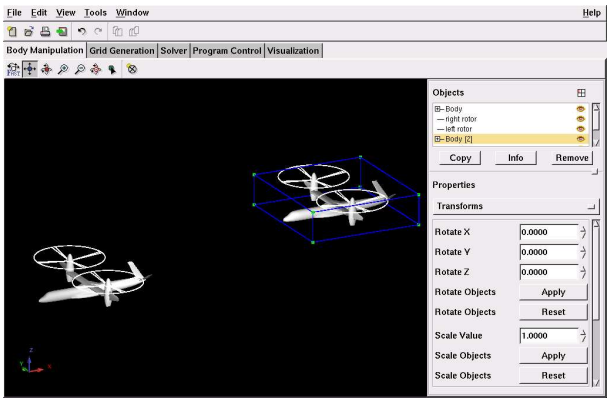

Figure 4: Formation of two LCTRs.

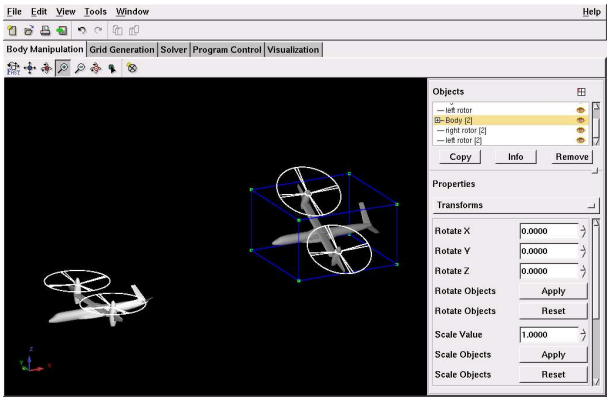

Figure 5: LCTR formation after rotation of rear aircraft.

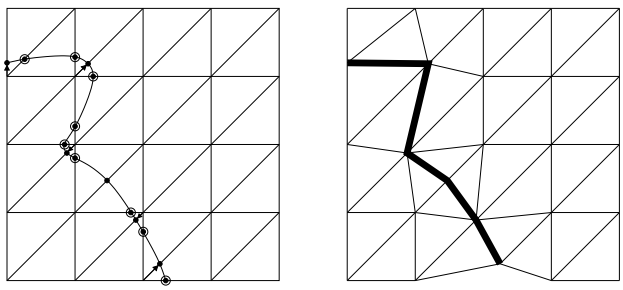

Figure 6: Body conforming grid example.

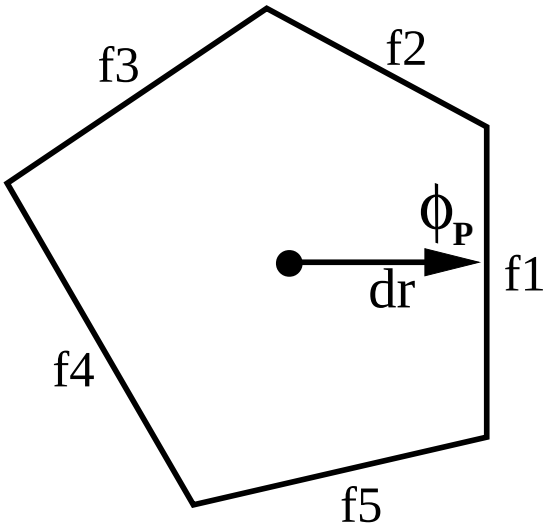

Figure 7: General unstructured control-volume.

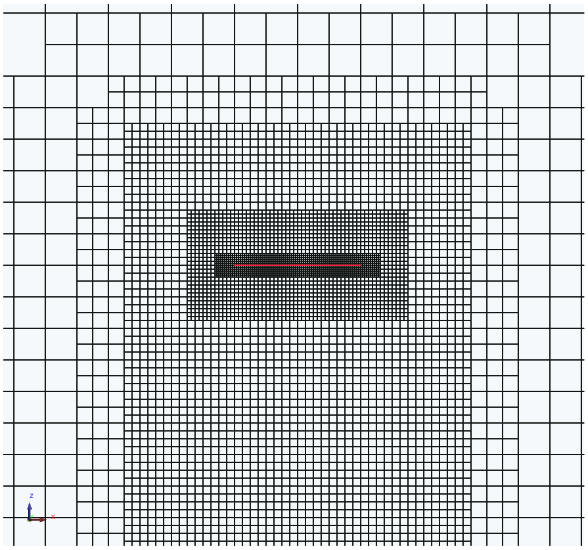

Figure 9: Sample RotCFD grid around the rotor.

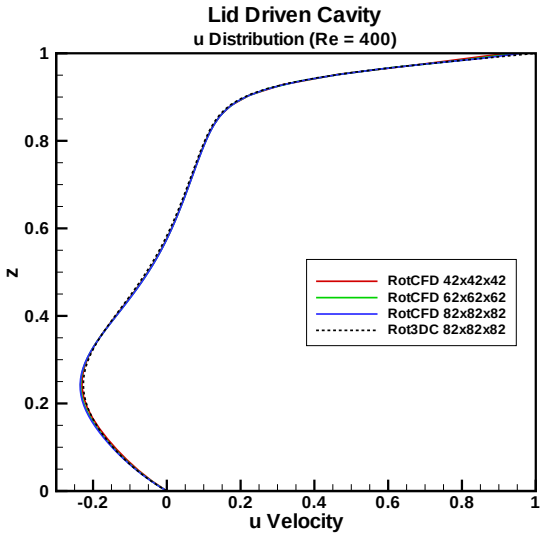

Figure 8: Centerline velocity profiles, $Re = 400$.

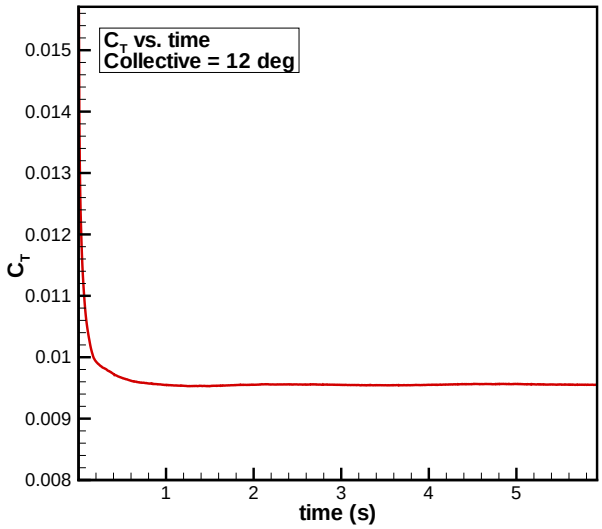

Figure 10: Variation of thrust coefficient with time, Rotor-I, Ref. [7].

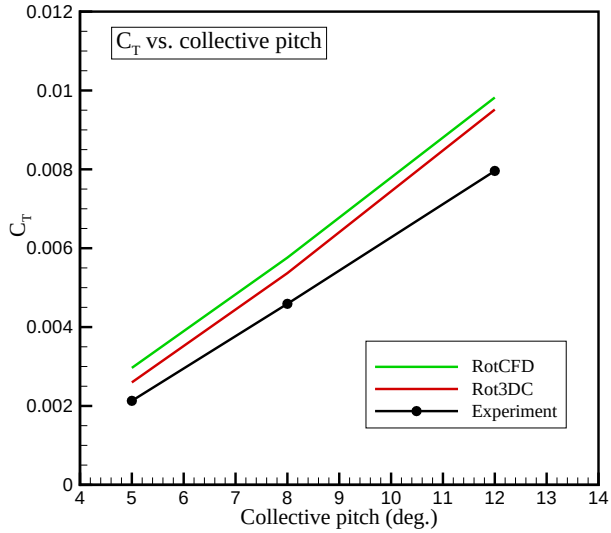

Figure 11: Correlation of thrust coefficient with collective pitch, Rotor-I, Ref. [7].

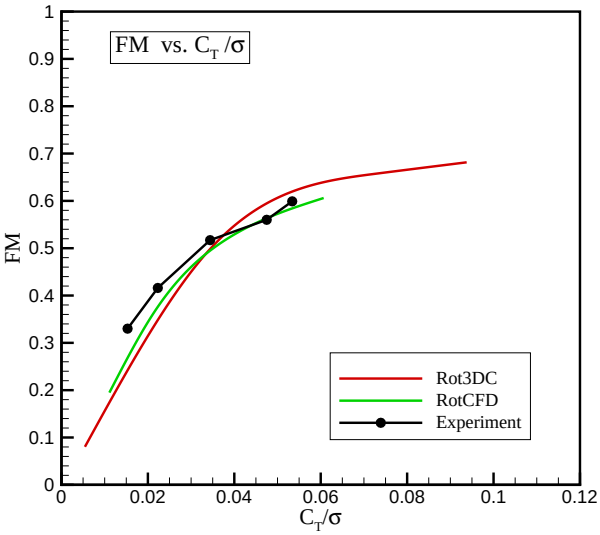

Figure 13: FM vs. C_T, Rotor-II, Ref. [8].

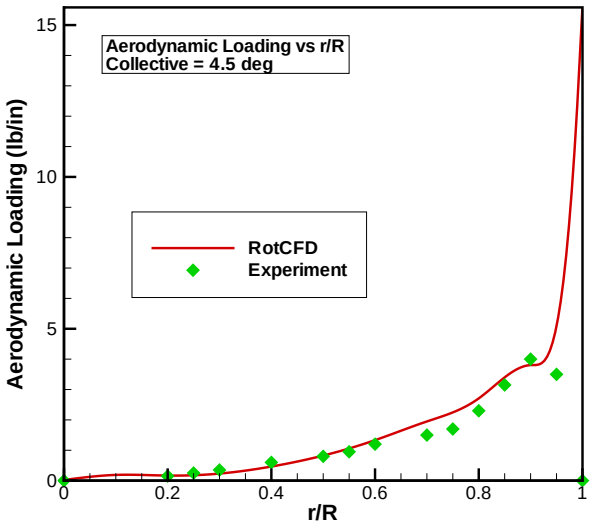

Figure 12: Spanwise aerodynamic loading, Rotor-II, Ref. [8].

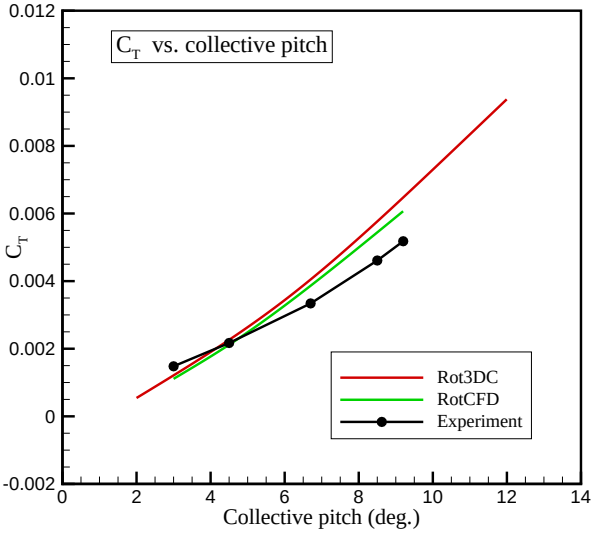

Figure 14: Correlation of thrust coefficient at collective pitch, Rotor-II, Ref. [8].

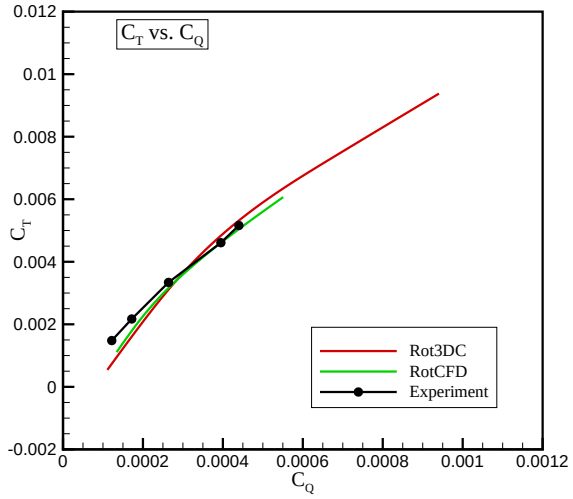

Figure 15: C_T vs. C_Q, Rotor-II, Ref. [8].

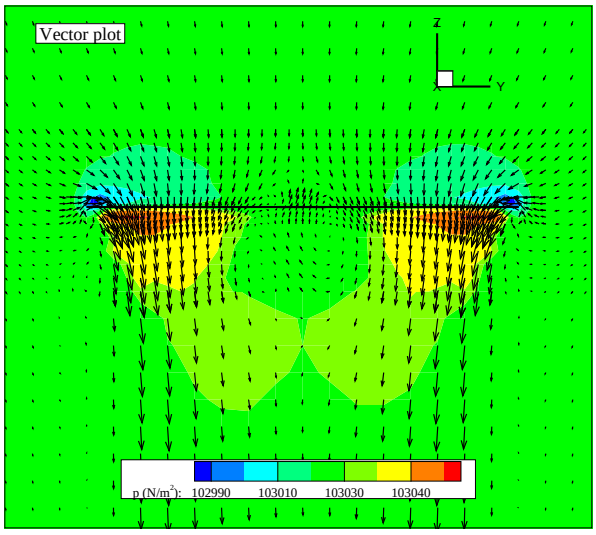

Figure 16: Pressure contours, Rotor-II, Ref. [8].

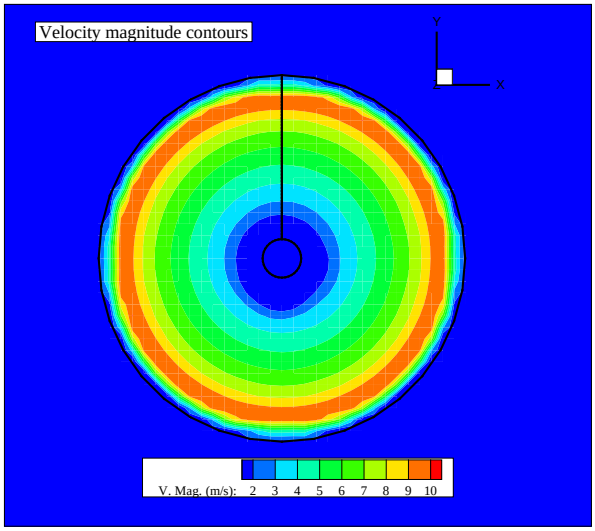

Figure 17: Velocity magnitude on the rotor plane, Rotor-II, Ref. [8].

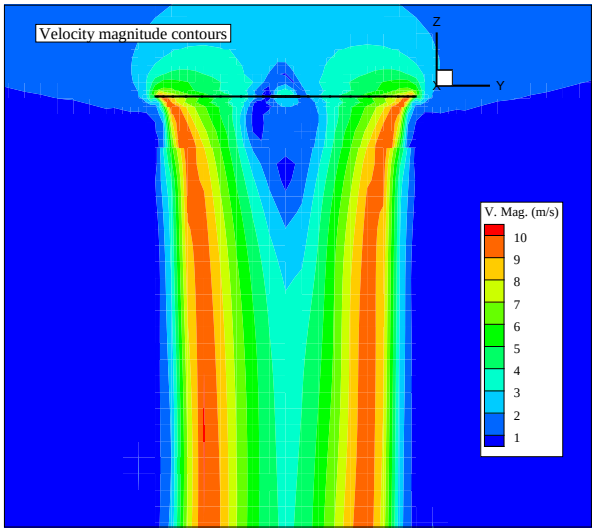

Figure 18: Velocity magnitude on x-plane through rotor center, Rotor-II, Ref. [8].

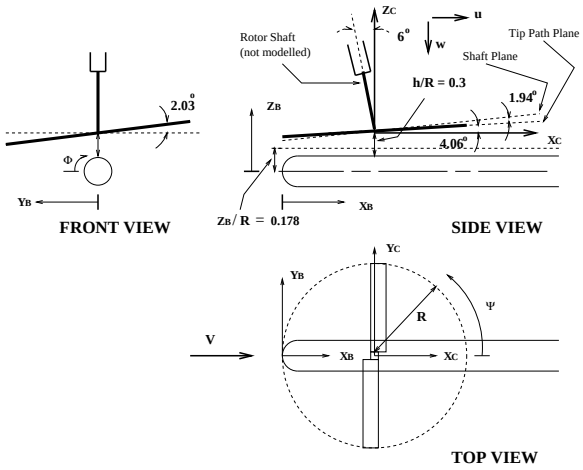

Figure 19: Geometry of simple body with 2 blded rotor, (Refs. [9], [11]).

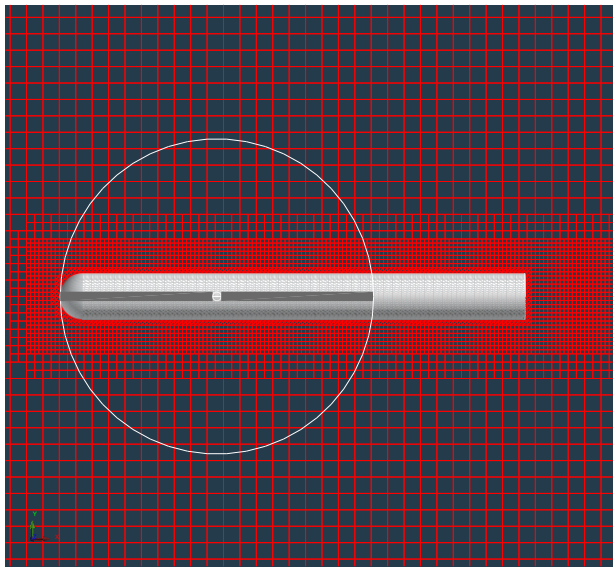

Figure 21: Z-plane view of the grid.

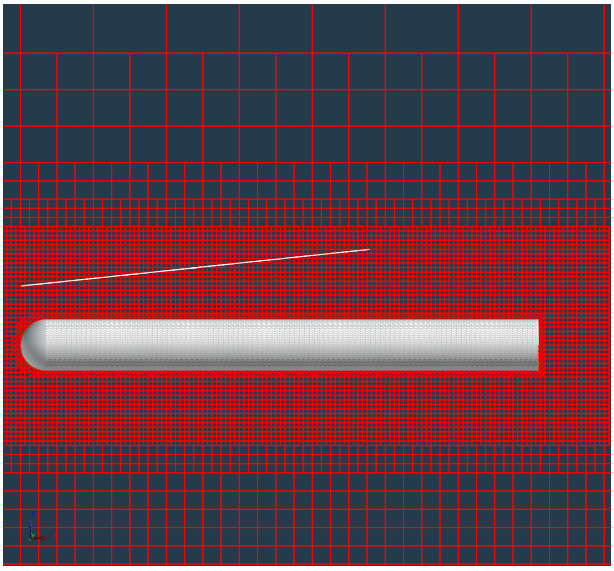

Figure 20: Y-plane view of the grid.

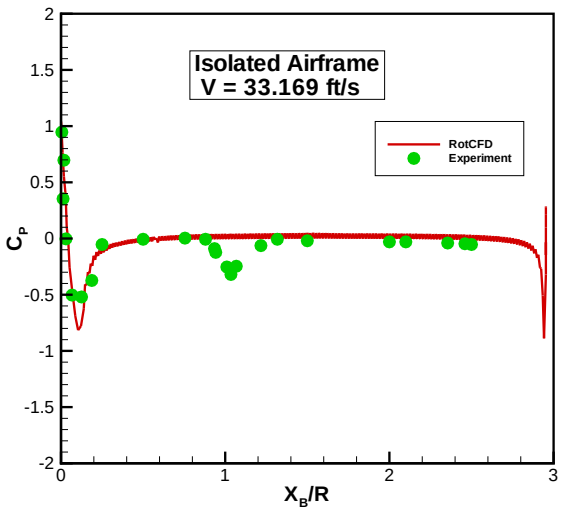

Figure 22: C_P distribution over an isolated airframe, $V_\infty = 33.169$ ft/s.

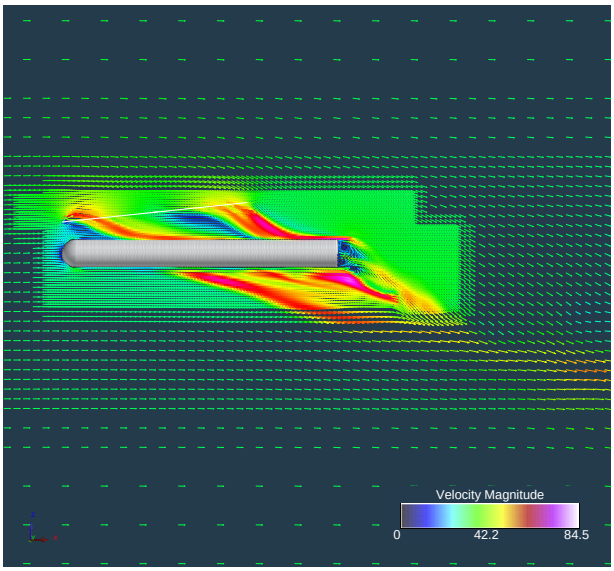

Figure 23: Velocity vector field at Y=0, $\mu = 0.1$.

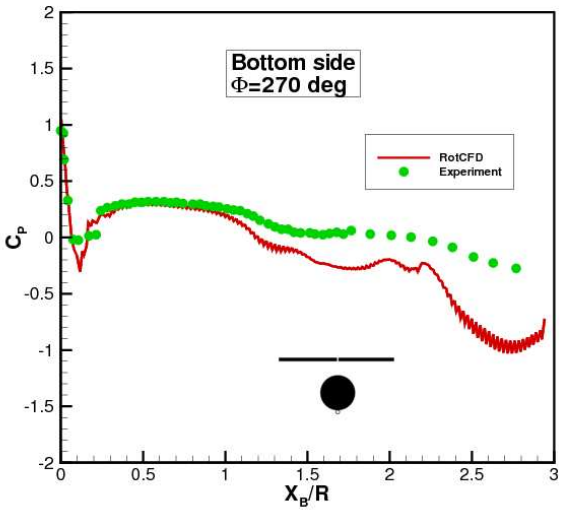

Figure 25: C_P distribution along bottom of body, $\mu = 0.1$.

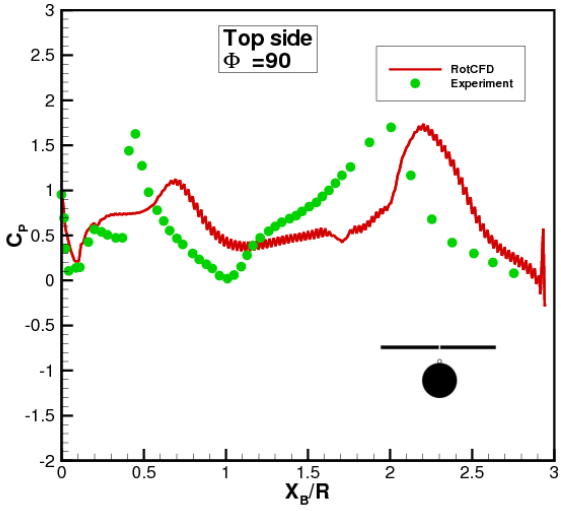

Figure 24: C_P distribution along top-centerline of body, $\mu = 0.1$.

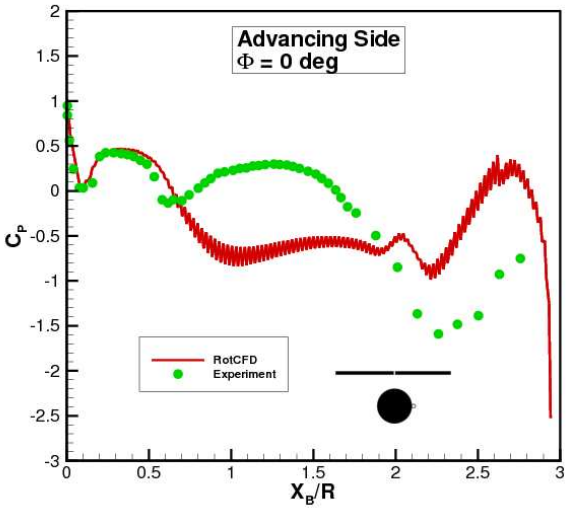

Figure 26: C_P distribution along advancing-blade side of body, $\mu = 0.1$.

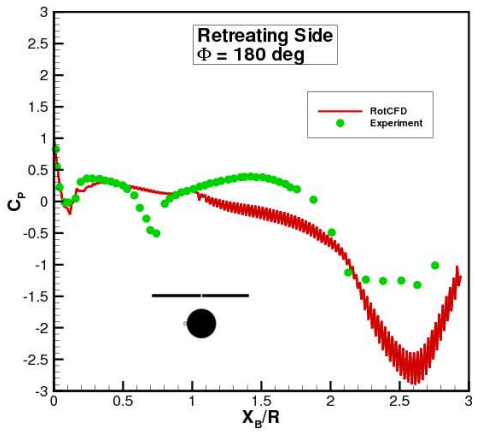

Figure 27: C_P distribution along retreating-blade side of body, $\mu = 0.1$.

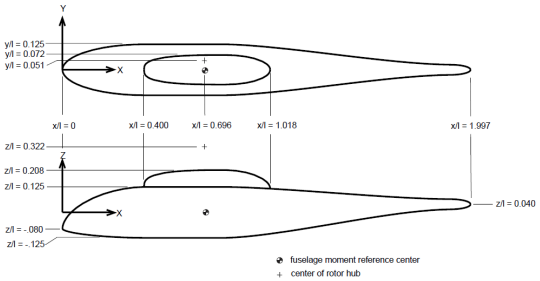

Figure 28: Rotor and body configuration [10].

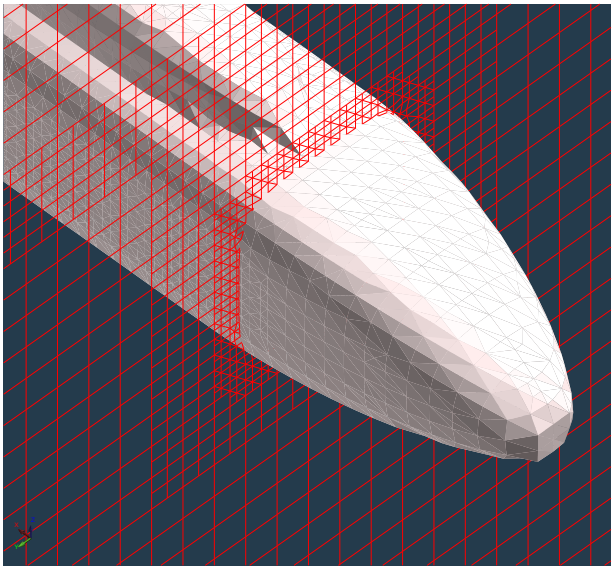

Figure 29: Detail of grid-body intersection.

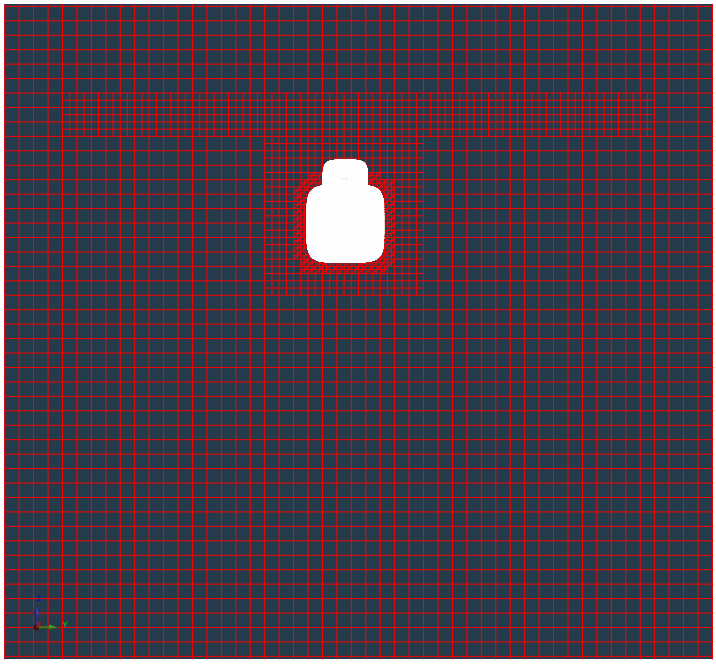

Figure 30: Grid-body intersection (X-plane cut).

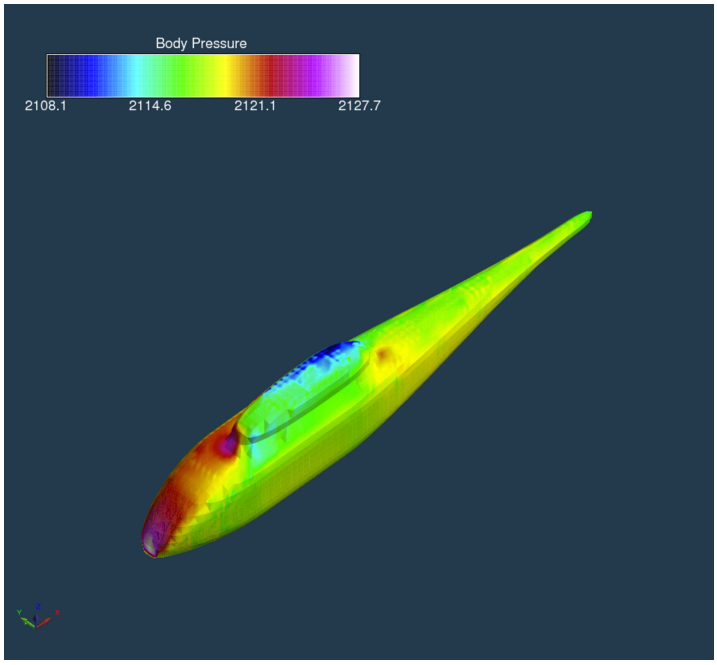

Figure 31: Rotor-body interaction, body pressure distribution.

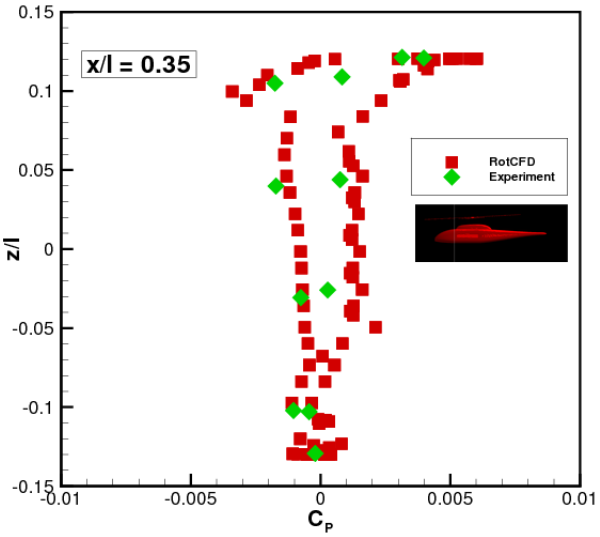

Figure 32: C_P distribution at 0.35l.

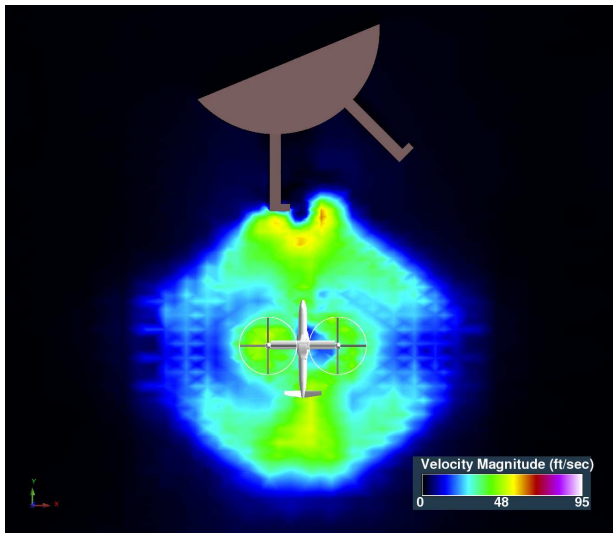

Figure 34: LCTR2 operating near a terminal.

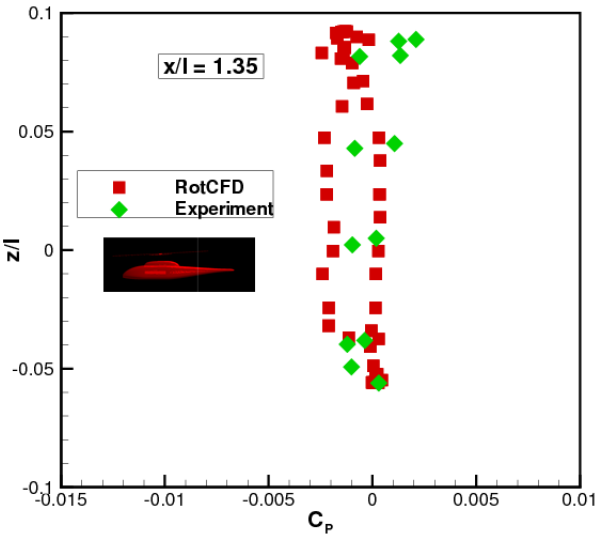

Figure 33: C_P distribution at 1.35l.

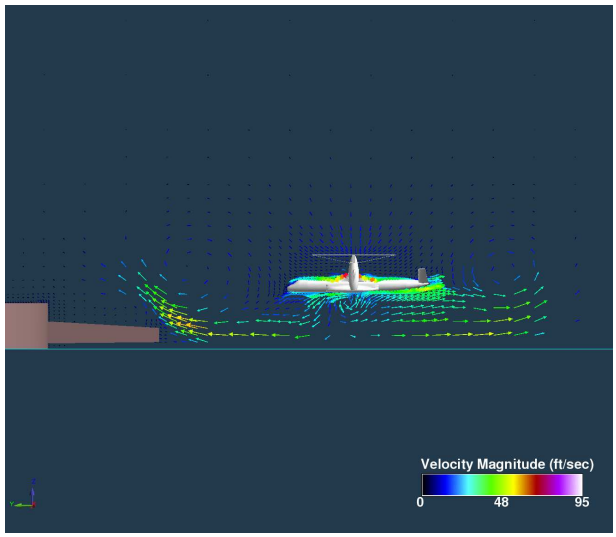

Figure 35: Vector field of LCTR2 near a terminal.

Table 1: Summary of Test Cases

	Case 1	Case 2
Rotor	Rotor-I, Ref. [7]	Rotor-II, Ref. [8]
$V_\infty, m/sec$	0.1	0.1
$V_{tip}, m/sec$	149.58	151.3
$\Omega_{tip}, rad/sec$	130.83	65.1
T, sec	0.048	0.097
ρ_∞, kg/m^3	1.225	1.225

Table 2: Rotor Geometric Properties

	Rotor-I	Rotor-II
Rotor radius, R (m)	1.143	2.3241
Chord, c (m)	0.191	0.36
Number of blades, N_b	2	2
Col. Pitch, θ_c (deg.)	5-12	3-9.2
Washout, θ_{tw} (deg.)	0	0
Root cutout	0.19R	0.15R
Hinge offset	0.0925R	0
Solidity, $N_b c/\pi R$	0.106	0.099
Airfoil	NACA-0012	NACA-0012

Table 3: Average C_T, Rotor-I, Ref. [7]

Col. Pitch	RotCFD	Rot3DC	Exp.
5^o	0.002965	0.002597	0.00213
8^o	0.005761	0.005368	0.00459
12^o	0.009821	0.009516	0.00796

Table 4: Average C_T, Rotor - II, Ref. [8]

Col. pitch	RotCFD C_T	Rot3DC C_T	Exp. C_T
3^o	0.001109	0.001203	0.00148
4.5^o	0.002118	0.002192	0.00217
6.7^o	0.003863	0.004087	0.00334
9.2^o	0.006069	0.006495	0.00518

Table 5: Rotor/airframe geometric characteristics (Refs. [9], [11])

Rotor radius	1.500 ft
Chord	0.2822 ft
Hub radius	0.041 ft
Hinge offset	0.0000 ft
Number of Blades	2
Washout	0.00 deg.
Collective pitch	10.0 deg.
Airfoil	NACA 0015
Airframe length	4.43 ft
Airframe diameter	0.44 ft
Rotor/airframe clearance*	0.443 ft

$*$ measured from rotor center to airframe surface

Table 6: Forward flight test conditions for rotor/airframe configuration, Ref. [9], Table[2]

μ	0.100
V_∞, ft/s	33.169
V_{tip}, ft/s	329.867
ω, rad/s	219.911
ρ, slugs/ft^3	0.002477
$\alpha_{s_{long}}$, deg.	-6.0
$\alpha_{s_{lat}}$, deg.	0.0
β_{1c}, deg.	0.0
β_{1s}, deg.	0.0
β_{2c}, deg.	-1.94
β_{2s}, deg.	-2.93

References

[1] S. V. Patankar. *Numerical Heat Transfer and Fluid Flow.* Hemisphere Publishing Corp, New York, 1980.

[2] S. R. Mathur and J. Y. Murthy. A pressure-based method for unstructured meshes. pages 166–180. 10th CFD Conference, 1991.

Table 7: Rotor Geometric Properties, Ref. [10]

Rotor radius, R (ft)	2.823
Chord, c (ft)	0.2175
Number of blades, N_b	4
Collective Pitch, θ_c (deg.)	10.3
Linear twist, θ_{tw} (deg.)	-8 deg
Root cutout	0.24R
Hinge offset	0.06R
Solidity, $N_b c/\pi R$	0.098
Airfoil	NACA-0012
Rotor shaft angle of attack	-3 deg
Cyclic Pitch Coefficient (A_1)	-2.7 deg
Cyclic Pitch Coefficient (B_1)	2.4 deg

Table 8: Flight Condition, Ref. [10]

$V_\infty, ft/sec$	89.36
$V_{tip}, ft/sec$	591
Ω_{tip}, rpm	2000
ρ_∞, slugs/ft^3	0.002377

[3] S. S. Ochs. *An Adaptively-Refined Quadtree Grid Method for Incompressible Flows*. PhD thesis, Iowa State University, 1998.

[4] R. G. Rajagopalan and C. K. Lim. Laminar flow analysis of a rotor in hover. *Journal of the American Helicopter Society*, 36:12–23, 1991.

[5] R. G. Rajagopalan and S. Mathur. Three dimensional analysis of a rotor in forward flight. *Journal of the American Helicopter Society*, 38:14–25, 1993.

[6] L. Zori and R. G. Rajagopalan. Navier-Stokes calculations of rotor-airframe interaction in forward flight. *Journal of the American Helicopter Society*, 40:57–67, 1995.

[7] F. X. Caradonna and C. Tung. Experimental and analytical studies of a model helicopter in hover,. *NASA Technical Memorandum, Note 81232*, September 1981.

[8] J. P. Rabbot Jr. Static-thrust measurements of the aerodynamic loading on a helicopter rotor blade,. *Langley Aeronautical Laboratory, Langley Field, VA., Technical Note 3688*, July 1956.

[9] A. G. Brand, N. M. Komerath, and H. M. McMahon. Wind tunnel data from a rotor wake/airframe interaction study. *School of Aerospace Engineering, Georgia Institute of Technology, Contract No. DAAG29-82-K-0094*, July 1986.

[10] R. E. Mineck and S. A. Gorton. Steady and periodic pressure measurements on a generic helicopter fuselage model in the presence of a rotor. *NASA/TM-2000-210286*, June 2000.

[11] L. A. J. Zori. Three-dimensional navier stokes calculations of a rotor/airframe interaction in forward flight. *M.S. Thesis, Iowa State University*, 1991.